Tailoring room temperature photoluminescence of antireflective silicon nanofacets

Tanmoy Basu, M. Kumar, A. Kanjilal, J. Ghatak, P. K. Sahoo, and T. Som

---

Articles you may be interested in

Absence of quantum confinement effects in the photoluminescence of Si3N4–embedded Si nanocrystals
J. Appl. Phys. **115**, 204301 (2014); 10.1063/1.4878699

Minimizing scattering from antireflective surfaces replicated from low-aspect-ratio black silicon
Appl. Phys. Lett. **101**, 131902 (2012); 10.1063/1.4754691

Surface modification of monocrystalline zinc oxide induced by high-density electronic excitation
J. Appl. Phys. **110**, 124310 (2011); 10.1063/1.3671006

Temperature and size dependence of time-resolved exciton recombination in ZnO quantum dots
Appl. Phys. Lett. **99**, 243107 (2011); 10.1063/1.3669511

Analysis of the stretched exponential photoluminescence decay from nanometer-sized silicon crystals in SiO 2
J. Appl. Phys. **86**, 6128 (1999); 10.1063/1.371663

CrossMark
click for updates

Tailoring room temperature photoluminescence of antireflective silicon nanofacets

Tanmoy Basu,[1] M. Kumar,[1] A. Kanjilal,[2] J. Ghatak,[1,a)] P. K. Sahoo,[3] and T. Som[1,b)]

[1]*Institute of Physics, Schivalaya Marg. Bhubaneswar 751 005, India*
[2]*Department of Physics, School of Natural Sciences, Shiv Nadar University, Gautam Budh Nagar, Uttar Pradesh 201 314, India*
[3]*National Institute of Science Education and Research, Bhubaneswar 751 005, India*

In this paper, a fluence-dependent antireflection performance is presented from ion-beam fabricated nanofaceted-Si surfaces. It is also demonstrated that these nanofacets are capable of producing room temperature ultra-violet and blue photoluminescence which can be attributed to inter-band transitions of the localized excitonic states of different Si-O bonds at the Si/SiO$_x$ interface. Time-resolved photoluminescence measurements further confirm defect-induced radiative emission from the surface of silicon nanofacets. It is observed that the spectral characteristics remain unchanged, except an enhancement in the photoluminescence intensity with increasing ion-fluence. The increase in photoluminescence intensity by orders of magnitude stronger than that of a planar Si substrate is due to higher absorption of incident photons by nanofaceted structures. © 2014 AIP Publishing LLC. [http://dx.doi.org/10.1063/1.4896069]

I. INTRODUCTION

Silicon nanostructures have drawn a lot of attention in recent years because of its unusual quantum confinement (QC) properties which yields unique structural, optical, and electronic behaviours,[1] viz. single electron devices,[2] sensors,[3] and cold cathodes for field-emission displays.[4] In bulk silicon, direct inter-band transitions are not allowed by the momentum conservation law and to make this happen, phonon absorption is required.[5] An alternative way to overcome this difficulty is to modify the electron dispersion equations for valence and conduction bands by controlling the size of Si nanostructures.[6] Besides QC-mediated photoluminescence (PL), Si-O defect states (generally exist at the surface of Si nanoclusters or at the Si/SiO$_x$ interface) also take part in radiative emission, as reported earlier.[7–9] Although the origin of PL emission from silicon nanostructures is a much debatable topic, silicon based ultraviolet (UV)-emitting materials always draw special attention since optical data storage devices often need light sources with shorter wavelengths, preferably in the UV range, for improving the storage density.

Over the last two decades, different types of Si-based nanocrystalline materials were prepared which exhibit PL comparable to porous silicon.[10] Although most of these studies are based on luminescence in the visible range, few studies exist where blue and UV light emission from Si nanostructures are addressed.[11,12] Despite much progress in the fabrication and luminescence property of Si nanostructures, one of the key challenges is to improve the emission efficiency which is largely dependent on the absorbed photons. Different approaches are followed to improve light extraction ratio (which in turn enhances the luminescence efficiency) by using photonic crystal structures, surface plasmon polariton etc.[13–15] However, these processes are complex and involve multiple fabrication steps. On the other hand, an alternative way to enhance absorption of light and in turn achieve higher emission efficiency is to use textured/rough surfaces which are effective to reduce reflection loss, leading to an improved light extraction ratio.[16,17] In fact, for a planar surface, a large difference in the refractive index between Si and air causes enhanced Fresnel reflection of the incident light from air to the substrate. This makes a diminishing intensity of the incident light available for absorption, leading to a large optical loss. In contrast, this loss gets minimized for textured surfaces—inspired by biomimetic moth-eye structures—where the surface micro/nano-structures lead to a gradual change in the effective refractive index between air and the substrate.[18] Recently, successful attempts have been made to fabricate light emitting diodes based on nanostructured surfaces where light extraction efficiency is seen to be enhanced.[19–21]

Ion-beam sputtering is known to be a single step processing route for pattern formation on a broad range of materials over macroscopic areas which is fast, cost-effective, and has the potential for transcending the constraints of lithography for device fabrication.[22] It has been demonstrated that various (size tunable) surface morphologies evolve on various types of materials, viz. metals,[23] semiconductors,[24,25] and insulators[26] depending on incidence angle, ion-energy, -flux, and -fluence. For obvious reasons, Si has been the most widely studied material for pattern formation using low energy ion beams.

In this paper, we emphasize on the importance of antireflection (AR) property of nanofaceted-Si surfaces, fabricated by low energy argon ions, to achieve tunable photoluminescence at room temperature (RT). Si surfaces having nanofacets of different heights were prepared at various ion fluences and two different angles of incidence, viz. 70° and

---

a)Present address: Jawaharlal Nehru Centre for Advanced Scientific Research, Bangalore 560 064, India.
b)Author to whom correspondence should be addressed. Electronic mail: tsom@iopb.res.in

72.5°. In both cases, the observed PL intensity from these nanostructures increases with ion fluence whereas an opposite trend is noticed for surface reflectance. Origin of such PL emission from the faceted-Si substrates is attributed to the argon-ion activated E' centres and Si-O related states present at the interface of Si/SiO_x. In particular, the observed PL peak at 370 nm has been correlated to the $-SiO_3$ group where the presence of different oxides at the surface has been confirmed by x-ray photoelectron spectroscopic (XPS) studies. Enhancement in the PL intensity has further been ascribed to the improved light absorption (i.e., reduction in surface reflectance) due to the presence of silicon nanofacets at the surface.

II. EXPERIMENTAL

Silicon samples, used in the present experiments, were sliced out $(1 \times 1 \, cm^2)$ from a *p*-type Si(100) wafer. A UHV-compatible experimental chamber (Prevac, Poland), equipped with an electron cyclotron resonance based broad beam ion source (Tectra GmbH, Germany), was used in this case. The chamber base pressure was below 5×10^{-9} mbar and the working pressure was maintained at 3×10^{-4} mbar. Substrates were fixed on the sample platen of 5-axes manipulator which was first covered by a sacrificial Si wafer (taken from the same lot of the substrate) to ensure a low impurity environment. Samples were exposed to 500 eV Ar-ions at two incidence angles, viz., $\theta = 70°$ and $72.5°$ (with respect to the surface normal) at RT. The beam diameter was measured to be 3 cm which corresponds to a fixed ion flux of 1.3×10^{14} ions cm^{-2} s^{-1} (corresponding to a target current of $160 \, \mu A$) in a plane normal to the ion-beam direction. Experiments were carried out for fluences ranging from 5×10^{17} to 2×10^{18} ions cm^{-2}.

Following Ar-ion exposure, the samples were imaged by *ex-situ* atomic force microscopy (AFM) [Asylum Research, USA]. All the AFM images were analyzed by using the WSxM software.[27] In addition, microstructural study was performed by using high-resolution transmission electron microscopy (HRTEM) [Jeol UHR 2010, Japan]. The surface chemical property was studied by XPS (VG instruments, UK) using Mg-K_α radiation source ($h\nu = 1254$ eV). Optical reflectance studies were carried out by using a UV-Vis-NIR spectrophotometer (Shimadzu-3101PC, Japan) at 45° incidence in the wavelength range of 300–800 nm. Room temperature PL measurements were performed at RT by steady state fluorescence spectrometer (Edinburgh instruments, USA) equipped with a 325 nm He-Cd laser (Kimmon, Japan).

III. RESULTS AND DISCUSSION

Figure 1 represents three-dimensional (3D) AFM topographic images obtained from samples after exposure to Ar-ions at $\theta = 70°$ and $72.5°$ at the highest ion fluence of 2×10^{18} ions cm^{-2}. It is observed that nanofaceted structures (conical) evolve up to 2×10^{18} ions cm^{-2}. Similar morphological evolution takes place for lower fluences as well (images not shown). Formation of such faceted morphology is observed only over this limited angular window.[28] Figure 1(c)
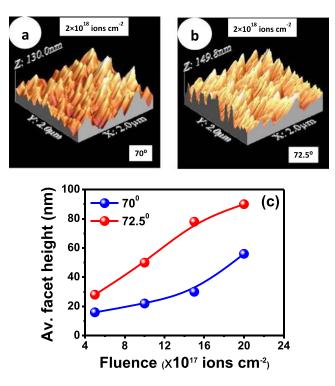

FIG. 1. Three-dimensional AFM micrographs corresponding to samples exposed to ion fluence of 2×10^{18} cm^{-2} at incidence angle of 70° (a) and 72.5° (b). (c) depicts the evolution of average facet heights as a function of ion fluence at $\theta = 70°$ and 72.5°.

depicts the evolution of average facet heights as a function of ion fluence at $\theta = 70°$ and $72.5°$ where an increasing trend is observed for both cases. Such nanofaceted structures evolve due to a transition from ripple (which are formed at fluences below 5×10^{17} ions cm^{-2}).[28] As a matter of fact, with an increase in the ratio of ripple height (h_0) to ripple wavelength (λ), the local angle of incidence along the ripple pattern eventually become so large that the upstream part of the ripple gets shadowed from the incoming ion-flux by the preceding peak. Thus, the limiting condition to avoid such shadowing of incident beam is[29]

$$\tan (\pi/2 - \theta) \geq 2\pi(h_0/\lambda),$$

where θ is the angle of incidence. According to this condition, if the ratio (h_0/λ) exceeds a threshold value, troughs of a sinusoid will not be eroded further but instead erosion will take place at the crest. This in turn can give rise to a faceted structure.[28]

In the present case, beyond the fluence of 2×10^{17} ions cm^{-2}, the condition of shadowing sets in and thus, it is expected to get faceted nanostructures as mentioned above. In addition, with increasing fluence, faceted nanostructures demonstrate coarsening behaviour. The observed facet coarsening is attributed to a mechanism based on reflection of primary ions from facets.[28,30] Recently, Engler *et al.* also reported formation of similar kind of faceted nanostructures on Si surface by using 2 keV Kr-ions at comparable fluences[31] and quantified the obtained faceted nanostructures in terms of facet height and slope distribution. It was demonstrated that with increasing ion fluence, the facet angle did not show any meaningful change. It may be mentioned that,
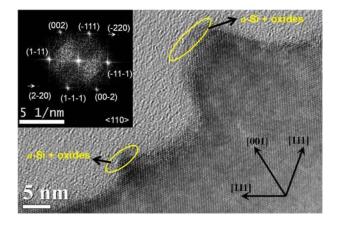
FIG. 2. XTEM image showing silicon facets fabricated by using 500 eV Ar-ions to the fluence of 5×10^{17} cm^{-2}. The black circles depict the zones where *a*-Si and native oxides are present. Inset shows the FFT of the same image which reveals presence of different crystallographic planes.

we also observed the similar trend for facet angle as a function of ion-fluence (the upstream facet angle becomes constant at 9° for both $\theta = 70°$ and 72.5°) by using the SPIP software.[32]

Microstructural investigations were also carried out by cross-sectional transmission electron microscopy (XTEM). Figure 2 depicts a high-resolution XTEM image of such a faceted surface which shows the clear presence of lattice fringes, indicating the formation of crystalline facets. A careful observation reveals the presence of amorphous patches (marked by yellow loops) around the apex of the facets, albeit they are absent along both the sidewalls. This was confirmed by looking at a large number of frames. These patches

may result from either ion induced amorphization of Si or the presence of native oxides.

In order to understand the fluence-dependent change in surface chemical properties, XPS studies were carried out for selective samples. Figures 3(a)–3(c) show the Si 2p spectra of pristine- and nanofaceted-Si samples exposed to the fluences of 5×10^{17} and 2×10^{18} ions cm^{-2} (for $\theta = 72.5°$). The Si 2p core level spectrum, corresponding to the pristine sample, shows the presence of silicon oxides (Si^{1+} in the form of SiO$_3$ and Si^{3+} in the form of Si$_2$O$_3$) along with some proportions of SiO$_2$ and Si-OH. The Si 2p spectrum corresponding to the fluence of 5×10^{17} ions cm^{-2} was deconvoluted into five peaks located at 98.25 ± 0.15, 99.77 ± 0.15, 101.59 ± 0.15, 102.97 ± 0.15, and 104.76 ± 0.15 eV which are assigned to Si, SiO$_3$, Si$_2$O$_3$, SiO$_2$, and Si-OH bonds, respectively.[33] On the other hand, O1s core level spectrum for the said fluence shows bonding with SiO$_x$ and H$_2$O. For the highest fluence of 2×10^{18} ions cm^{-2}, a similar trend is observed although Si concentration is little higher compared to that at the lowest fluence case. Relative amount of the respective components in the pristine and irradiated samples, determined from XPS analyses, are listed in Table I. The survey spectra (not shown) at all fluences did not reveal the presence of any Fe signal from nanofaceted samples. This is expected for the chosen experimental geometry where a sacrificial Si wafer was used to cover the entire sample platen (as described in the experimental section and Ref. 25) to avoid having impurity-induced nanostructure formation at such a glancing incidence angle. Similar results are obtained for $\theta = 70°$ (spectra not shown) as well. Thus, the amorphous patches at the facet apexes mostly consist of native oxide
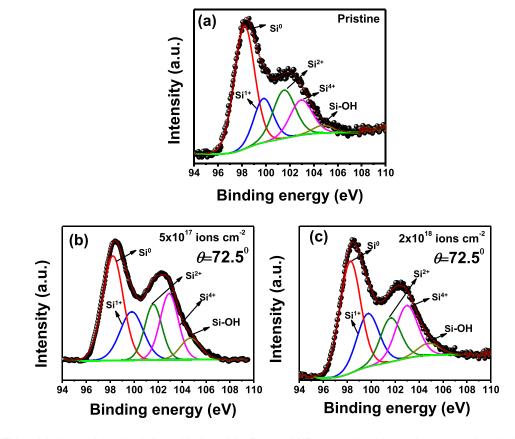

FIG. 3. 2p core level Si XPS spectra taken from (a) Pristine-Si and samples exposed to ion fluences of (b) 5×10^{17}, (c) 2×10^{18} cm^{-2}, respectively.

TABLE I. Chemical compositional analyses using XPS.

Sample	Binding energy (eV)	Chemical composition	Concentration (%)
Pristine-Si	98.2	Si^0, Si elemental	46.58
	99.78	Si^{1+}, SiO_3	15.92
	101.51	Si^{2+}, Si_2O_3	19.98
	102.94	Si^{4+}, SiO_2	14.61
	104.76	Si-OH	2.91
Si irradiated with 5×10^{17} Ar^+ cm^{-2} at 72.5°	98.22	Si^0, Si elemental	36.58
	99.79	Si^{1+}, SiO_3	19.19
	101.59	Si^{2+}, Si_2O_3	16.31
	102.92	Si^{4+}, SiO_2	20.51
	104.7	Si-OH	7.41
Si irradiated with 2×10^{18} Ar^+ cm^{-2} at 72.5°	98.24	Si^0, Si elemental	39.85
	99.72	Si^{1+}, SiO_3	20.22
	101.62	Si^{2+}, Si_2O_3	15.6
	102.97	Si^{4+}, SiO_2	19.74
	104.79	Si-OH	4.59

layer (SiO_x) which matches well with the prediction made on the basis of XTEM image shown in Fig. 2.

Figure 4(a) presents the change in surface reflectance with increasing ion fluence in the range of 5×10^{17} $- 2 \times 10^{18}$ ions cm^{-2} for $\theta = 72.5°$. It is observed that the reflectance decreases with increasing fluence. For instance, the reflectance at 550 nm reaches the values of 40% (for 5×10^{17} ions cm^{-2}), 38% (for 1×10^{18} ions cm^{-2}), and 26% (for 2×10^{18} ions cm^{-2}). A similar trend is observed (reflectance reduces up to 31% for the fluence 2×10^{18} ions cm^{-2}) in case of $\theta = 70°$ incidence angle (spectra not shown). Thus, it can be inferred that argon-ion induced topographically modulated Si surfaces (having faceted nanostructures) can manifest variable degree of AR property which is dependent on angle of incidence of ions and fluence. In order to correlate the change in AR property with the surface morphology observed at two different θ-values and Ar-ion fluences, we used SPIP software[32] to calculate the percentage area covered by the Si faceted structures with respect to air and plot it against the corresponding facet height at different fluences [Fig. 4(b)]. This shows an increasing trend in the surface height with decreasing percentage area covered by the facets. Thus, in our case, a faceted surface has a gradually varying Si-fraction from top (100% air: 0% Si) to bottom (0% air: 100% Si). This is further supported by the plots shown in Fig. 1(c) where facet height increases as a function of ion fluence. Since a gradual change in facet height leads to the gradual variation in percentage area covered by the facets from top (100% air: 0% Si) to bottom (0% air: 100% Si), the observed AR property of nanofaceted-Si substrates can be understood in terms of well-known graded refractive index effect.[34] Corresponding schematic diagram of the refractive index profile from air to Si substrate due to the presence of a facet is shown in Fig. 4(c) where the presence of small amount (as compared to total facet) of amorphous-Si and native oxides at the apex was neglected. This gradual variation in refractive index can effectively eliminate the reflected light across a wide spectrum.[34] In the present case, with increasing sputtering time, facet dimensions become larger
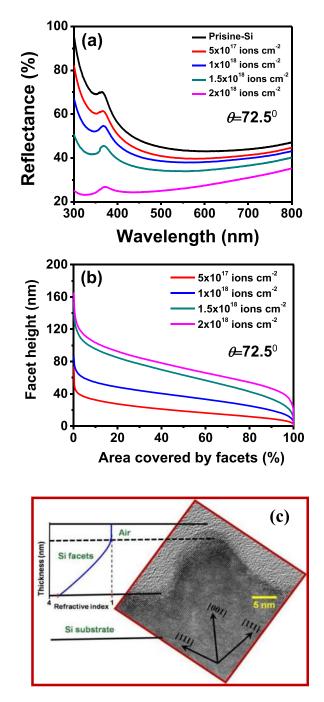

FIG. 4. (a) Reflectance study corresponding to pristine-Si and samples exposed to four different ion fluences, viz. 5×10^{17}, 1×10^{18}, 1.5×10^{18}, and 2×10^{18} cm^{-2} for incidence angle of 72.5°, (b) facet height versus percentage area covered by the faceted structures extracted by using SPIP software from the respective AFM images shown in Fig. 1, and (c) schematic of the refractive index profile from air to Si substrate due to the presence of a facet.

[as observed from Fig. 1(c)] which improves the antireflection over a wide spectral range.

The PL spectra of Si-nanofacets are presented in Fig. 5. In case of $\theta = 72.5°$, PL intensity is the weakest for the lowest fluence whereas it becomes the strongest at the highest fluence. It is observed that several PL peaks are located in the energy range of 3.39–2.67 eV (365–465 nm). Figure 5 illustrates that for the fluence of 5×10^{17} ions cm^{-2}, a small shoulder appears at 373.5 nm along with a clear peak at
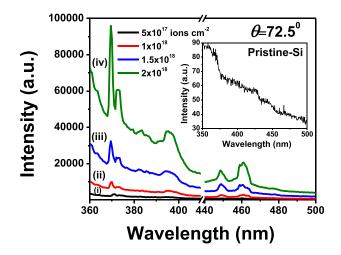
FIG. 5. PL spectra plotted against wavelength for ion incidence angle of 72.5° and for fluences of (i) 5×10^{17}, (ii) 1×10^{18}, (iii) 1.5×10^{18}, and (iv) 2×10^{18} ions cm^{-2}, respectively. Inset shows the PL spectrum corresponding to pristine-Si.

371 nm. With increasing fluence up to 2×10^{18} ions cm^{-2}, a blue shift ($\sim$2.5 nm) is observed which is accompanied by the appearance of a less intense peak is detected at 396 nm. The inset of Fig. 5 shows the PL spectrum of a pristine-Si sample where no other PL peak is observed except a small hump at around 370 nm. This indicates that the origin of 371 nm PL band, in our case (including pristine-Si), may be related to the native oxide layer formed on top of the crystalline-Si. For UV light emission from Si-based nanostructures, two possible mechanisms are proposed. One is based on quantum size effect, which says that the excitation occurs between the quantized levels of nanocrystallites and the recombination happens either directly between the same levels or at the nanocrystalline surface/interface states after a relaxation process.[35–38] The other possibility is the presence of Si-O related species which governs the whole excitation and recombination processes.[39–43]

To understand the origin of light emission from silicon nanostructures, we first explore the possibility of nanostructure-driven quantum confinement effect in silicon. For example, the model described by Zheng *et al.*[12] calculates the electronic states and optical transition matrix elements of Si quantum tips in a large energy range which yields transitions in the energy range of 2–4 eV. In another work, Adachi *et al.* reported UV PL emission at RT from porous silicon where they have attributed the results to the reduction in the E_1 critical point from two-dimension (2D) to zero-dimension (0D) due to quantum size effect.[44] As compared to silicon quantum tips or nanocrystals in case of faceted silicon, the apexes have the dimension in the range of 3–10 nm (Fig. 3) and they grow in the (001) direction. Thus, apparently, quantum confinement may play a role for the observed PL emission in the present case. In that case, one would expect a broad PL band due to a large distribution of the quantum tips and sizes. However, neither broadening nor blue shift of the PL peak in the UV region is observed in our case and hence, the possibility of quantum confinement in the present study may be ruled out. Thus, in our case, Si-O related defects seem to be more important for generating

light emission. The UV PL band at 365 nm (in our case 370 ± 2 nm) was attributed to the hole-trapped E' centres ($O_3 \equiv Si$) by Kim *et al.*[45] In this study, XPS measurements reveal the presence of E' centres in the form of $O_3 \equiv Si$ for both pristine and ion-irradiated samples and the corresponding concentrations are given in Table I. Although SiO_3 (concentration 18.76%) is present in pristine Si, it does not give rise to any strong 368 nm PL. On the other hand, one can strengthen this emission by exposing to 500 eV Ar-ions. Thus, it can be inferred that the E' centres become more active due to the presence of Si nanofacets formed under argon-ion exposure because of the increased surface-to-volume ratio of the nanofacets. The small peak that appears at $\sim$373 nm shows the similar behaviour and should be related to the same mechanism stated above.

Let us now try to explain the origin of the 396 nm emission from nanofaceted-Si structures. UV emission from porous silicon was reported earlier by Kanjilal *et al.*[46] where they reported on the 396 nm PL band and explained it on the basis of QC-luminescence centre (LC) model.[47] In addition, the role of fluorine related defects was also addressed. In the present case, we do not observe any fluorine related peak from XPS analysis which indicates that the observed emission at 396 nm should be related to the luminescence centres present in the vicinity of the silicon nanostructures. As mentioned by Qin *et al.*,[47] there is a possibility of lack of non-radiative recombination centres inside the nanoscale objects of Si and therefore, radiative recombination takes place through the luminescence centres present outside Si nanostructures. According to this, the light emission takes place in two steps: First, photo-excitation takes place inside Si nanostructures and subsequently the excited electrons and holes tunnel into the surrounding SiO_x layers.[47] Second, the electrons and holes recombine radiatively via LCs in the neighbourhood. The aforementioned discussion is also true in the present case, showing the PL signal at 396 nm for an excitation wavelength of 325 nm. As discerned from the XTEM image and XPS studies, the apexes of the faceted nanostructures are rich in SiO_x. Thus, the neutral oxygen vacancy sites located in the peripheral SiO_x (on the top of the Si facets) can work as the LCs and give rise to the near-UV emission. Another possible explanation would be the formation of interconnects with the crystalline-Si nanostructures due to the diffusion of oxygen atoms. Kanemitsu *et al.*[48] reported that in case of oxidized porous silicon, amorphous SiO_2 layer on crystalline-Si core may give rise to PL emission in the range of 310–413 nm. Actually, at the interface of SiO_2/Si, electronic states are created due to the presence of the amorphous layer. With increasing temperature, oxygen atoms can diffuse into the crystalline layer and subsequently form bridges or interconnected silicon atoms. According to Kanemitsu *et al.*, the inter-connected Si structure has a direct band gap of 3–4 eV which can give rise to blue light emission. Due to a large mismatch in the band gaps between interface and the outer surface, carriers may get confined in the Si-core. The same group reported that the corresponding blue emission decayed with a time constant of 650 ps.[48] Following this argument, we propose here that ion-exposure provides sufficient energy to oxygen atoms at the surface to

inter-diffuse in the silicon matrix and to form bridges which give rise to the 396 nm emission line (in case of all ion-irradiated samples). To validate our claim further, time-resolved PL measurements were performed at an excitation wavelength of 375 nm by using a pulsed diode laser corresponding to the peak observed at 396 nm. The time constant turns out to be 347 ps which is close to the value obtained in case of porous silicon.[48] Thus, in the present case, it is difficult to point out the dominant mechanism (for UV PL emission) between these two.

Apart from the above-mentioned PL bands, appearance of twin peaks in the blue (449 and 460 nm) region is observed explicitly in case of argon-ion irradiated Si samples. It may be mentioned that the PL band at 468 nm PL band is thoroughly studied in case of silica glass and ion implanted silicon.[49–51] This blue emission generally corresponds to the photo-absorption of neutral oxygen vacancies ($O_3 \equiv Si\text{-}Si \equiv O_3$) and diamagnetic radiative recombination centres.[52] Thus, oxygen vacancies can play a crucial role in generating blue light emission. Origin of oxygen vacancies in Si is governed by different factors. For instance, Friebele and Griscom showed that oxygen vacancies are generated from the energetic electrons in the ionization cascade during irradiation process.[53] In another study, Devine *et al.* discussed oxygen vacancy generation process during ion bombardment.[54] Absorption of photons of energy higher than the band gap of SiO_2 generates electron-hole pairs, a substantial portion of which gets converted to excitons. These excitons become the so-called self-trapped excitons when they get localized within the material by defects in the material. The radiative recombination of self-trapped excitons can produce blue (2.7 eV) PL emission.[54] Following the above discussion, oxygen vacancies generated during Ar-ion irradiation process might be acting as trap centres for photo-generated excitons in SiO_2 (as evident from XPS analysis). These trapped excitons subsequently recombine to give rise to PL bands at 449 and 460 nm.

The key result in the present case is the observation of drastic enhancement in overall PL intensity (at RT) as a function of ion-fluence. We explored the possibility of correlating this behaviour to the improved antireflection/enhanced absorption property of the nanofaceted-Si. This seems more plausible in our case as XPS analyses (Fig. 3) do not reveal much difference in the concentration of chemical species in the pristine and ion-irradiated Si samples. Thus, it is clear that the observed enhancement in the PL intensity is not due to the variation in the concentration of different defect states but something else. It has been reported that light extraction from Si-based materials can be enhanced by making use of textured surfaces which show enhanced luminescent property by surface roughening process.[21] As discussed above, the surface reflectance is significantly suppressed by using nanopatterned structures (Fig. 4), the light emission should effectively increase due to the antireflection effect over a wide spectral range. Since the reflection of incident light in the UV region also reduces [as observed from Fig. 4(a)], the more incident light can be absorbed in the Si nanofacets to excite much more electron-hole pairs leading to a stronger emission. It may be noted that the excitation wavelength

(325 nm) is in the UV region and from the reflectance measurements [Fig. 4(a)], we observe a significant improvement in the AR property as a function ion fluence, in the UV region as well. Thus, the excitation light (He-Cd laser, 325 nm) gets benefited from this antireflection property and maximum increment in the emission intensity is observed in the spectral range of 360–380 nm. Thus, the improved AR property of nanofaceted-Si contributes to the significant enhancement in the PL intensity particularly in the UV region.

IV. CONCLUSIONS

In conclusion, an ion-fluence dependent tunable room temperature PL emission is demonstrated from nanofaceted-Si structures produced by 500 eV argon ion bombardment at oblique incidences. Origin of this UV PL emission is explained by taking into account argon-ion activated E' centres and Si-O related states present at the interface of Si/SiO_x nanofacets. On the other hand, emission in the blue region corresponds to the self-trapped excitons localized at the argon-ion induced oxygen vacancies at the surface of crystalline nanofacets. The enhancement in the overall PL intensity is attributed to the decrease in surface reflectance as a function of fluence due to the presence of textured surfaces (decorated with nanofacets). Thus, our experimental results show that the intensities of light emission of Si-based devices can be improved by using nanoscale textured surfaces. The present study indicates that silicon nanofacets might be a good candidate both as a functional silicon nanostructure and as a template for assembling silicon-based nanocomposites in fabricating optoelectronic nanodevices.

ACKNOWLEDGMENTS

[1]J. M. Garguilo, F. A. M. Koeck, R. J. Nemanich, X. C. Xiao, J. A. Carlisle, and O. Auciello, Phys. Rev. B **72**, 165404 (2005).

[2]S. Fujita, K. Uchida, S. Yasuda, R. Ohba, and T. Tanamoto, Nanotech. **3**, 309 (2003).

[3]M. W. Shao, Y. Y. Shan, N. B. Wong, and S. T. Lee, Adv. Funct. Mater. **15**, 1478 (2005).

[4]M. Kanechika, N. Sugimoto, and Y. Mitsushima, J. Appl. Phys. **98**, 054907 (2005).

[5]R. Tsu and K. Daneshvar, ECS Trans. **2**, 1 (2007).

[6]A. P. Alivisatos, Science **271**, 933 (1996).

[7]N. Daldosso, M. Luppi, S. Ossicini, E. Degoli, R. Magri, G. Dalba, P. Fornasini, R. Grisenti, F. Rocca, L. Pavesi, S. Boninelli, F. Priolo, C. Spinella, and F. Iacona, Phys. Rev. B **68**, 085327 (2003).

[8]G.-R. Lin, C.-J. Lin, C.-K. Lin, L.-J. Chou, and Y.-L. Chueh, J. Appl. Phys. **97**, 094306 (2005).

[9]F. Iacona, G. Franzò, and C. Spinella, J. Appl. Phys. **87**, 1295 (2000).

[10]X. Wen, L. Van Dao, and P. Hannaford, J. Phys. D: Appl. Phys. **40**, 3573 (2007).

[11]G. Sahu, H. P. Lenka, D. P. Mahapatra, B. Rout, and M. P. Das, Adv. Nat. Sci.: Nanosci. Nanotechnol. **3**, 025002 (2012).

[12]W. H. Zheng, J.-b. Xia, S. D. Lam, K. W. Cheah, M. R. Rakhshandehroo, and S. W. Pang, Appl. Phys. Lett. **74**, 386 (1999).

[13]Y. Mochizuki, M. Fujii, S. Hayashi, T. Tsuruoka, and K. Akamatsu, J. Appl. Phys. **106**, 013517 (2009).

[14]J. Goffard, D. Gérard, P. Miska, A.-L. Baudrion, R. Deturche, and J. Plain, Sci. Rep. **3**, 2672 (2013).

[15]B. Kim, C. Cho, J. Mun, M. Kwon, T. Park, J. S. Kim, C. C. Byeon, J. Lee, and S. Park, Adv. Mater. **20**, 3100 (2008).
[16]M. Hsieh, C. Wang, L. Chen, T. Lin, M. Ke, Y. Cheng, Y. Yu, C. Chen, D. Yeh, C. Lu, C. Huang, C. Yang, and J. Huang, IEEE Electron Device Lett. **29**, 658 (2008).
[17]P. Lalanne and G. M. Morris, Nanotechnology **8**, 53 (1997).
[18]Y.-F. Huang, S. Chattopadhyay, Y.-J. Jen, C.-Y. Peng, T.-A. Liu, Y.-K. Hsu, C.-L. Pan, H.-C. Lo, C.-H. Hsu, Y.-H. Chang, C.-S. Lee, K.-H. Chen, and L.-C. Chen, Nat. Nanotechnol. **2**, 770 (2007).
[19]A. O. Altun, S. Jeon, J. Shim, J.-H. Jeong, D.-G. Choi, K.-D. Kim, J.-H. Choi, S.-W. Lee, E.-S. Lee, and H.-D. Park, Org. Electron. **11**, 711 (2010).
[20]A. C. Tamboli, K. C. McGroddy, and E. L. Hu, Phys. Status Solidi C **6**, S807 (2009).
[21]Y. Liu, J. Xu, H. Sun, S. Sun, W. Xu, L. Xu, and K. Chen, Opt. Express **19**, 3347 (2011).
[22]T. Som and D. Kanjilal, *Nanofabrication by Ion-Beam Sputtering: Fundamentals and Applications* (Pan Stanford, Singapore, 2012).
[23]M. Stepanova, S. K. Dew, and I. P. Soshnikov, Appl. Phys. Lett. **86**, 073112 (2005).
[24]S. Facsko, T. Dekorsy, C. Koerdt, C. Trappe, H. Kurz, A. Vogt, and H. L. Hartnagel, Science **285**, 1551 (1999).
[25]T. Basu, J. R. Mohanty, and T. Som, Appl. Surf. Sci. **258**, 9944 (2012).
[26]M. O. Liedke, M. Körner, K. Lenz, F. Grossmann, S. Facsko, and J. Fassbender, Appl. Phys. Lett. **100**, 242405 (2012).
[27]See http://www.nanotec.es/products/wsxm/index.php.
[28]T. Basu, D. P. Datta, and T. Som, Nanoscale Res. Lett. **8**, 289 (2013).
[29]G. Carter, J. Appl. Phys. **85**, 455 (1999).
[30]W. Hauffe, Phys. Status Solidi A **35**, K93 (1976).
[31]M. Engler, S. Macko, F. Frost, and T. Michely, Phys. Rev. B **89**, 245412 (2014).
[32]See http://www.imagemet.com/index.php?main=products.
[33]F. G. Bell and L. Ley, Phys. Rev. B **37**, 8383 (1988).
[34]W. H. Southwell, Opt. Lett. **8**, 584 (1983).
[35]D. J. Lockwood, Z. J. Lu, and J.-M. Baribeau, Phys. Rev. Lett. **76**, 539 (1996).
[36]E. Edelberg, S. Bergh, R. Naone, M. Hall, and E. S. Aydil, Appl. Phys. Lett. **68**, 1415 (1996).
[37]S. Tong, X. Liu, and X. Bao, Appl. Phys. Lett. **66**, 469 (1995).
[38]X.-N. Liu, S. Tong, L.-C. Wang, G.-X. Chen, and X.-M. Bao, J. Appl. Phys. **78**, 6193(1995).
[39]L. Skuja, J. Non-Cryst. Solids **149**, 77 (1992).
[40]L. Lucovsky, Philos. Mag. **39**, 513 (1979).
[41]C. M. Gee and M. Kastner, Phys. Rev. Lett. **42**, 1765 (1979).
[42]D. L. Griscom, J. Non-Cryst. Solids **73**, 51(1985).
[43]E. P. O'Reilly and J. Robertson, Phys. Rev. B **27**, 3780 (1983).
[44]S. Adachi, T. Miyazaki, K. Inoue, and S. Sodezawa, Jpn. J. Appl. Phys. **46**, 4028 (2007).
[45]K. Kim, M. S. Suh, T. S. Kim, C. J. Youn, E. K. Suh, Y. J. Shin, K. B. Lee, and H. J. Lee, Appl. Phys. Lett. **69**, 3908 (1996).
[46]A. Kanjilal, M. Song, K. Furuya, and B. Mallik, J. Phys. D: Appl. Phys. **40**, 5044 (2007).
[47]C. G. Qin and Y. Q. Jia, Solid State Commun. **86**, 559 (1993).
[48]Y. Kanemitsu, T. Futagi, T. Matsumoto, and H. Mimura, Phys. Rev. B **49**, 14732 (1994).
[49]R. Tohmon, Y. Shimogaichi, H. Mizuno, Y. Ohko, K. Nagasawa, and Y. Hama, Phys. Rev. Lett. **62**, 1388 (1989).
[50]H. Nishikawa, T. Shiroyama, R. Nakamura, Y. Ohki, K. Nagasawa, and Y. Hama, Phys. Rev. B **45**, 586 (1992).
[51]H. Z. Song and X. M. Bao, Phys. Rev. B **55**, 6988 (1997).
[52]C. G. Siu, X. L. Wu, and X. M. Bao, Appl. Phys. Lett. **74**, 1812 (1999).
[53]E. J. Friebele and D. L. Griscom, in *Treatise on Materials Science and Technology*, edited by M. Tomozawa and R. H. Doremus (Academic, New York, 1979), Vol. 17, p. 257.
[54]R. A. B. Devine, Appl. Phys. Lett. **43**, 1056 (1983).